

MINIMUM DUST ABUNDANCES FOR PLANETESIMAL FORMATION VIA SECULAR GRAVITATIONAL INSTABILITIES

TAKU TAKEUCHI¹ AND SHIGERU IDA

Department of Earth and Planetary Sciences, Tokyo Institute of Technology, Meguro-ku, Tokyo, 152-8551, Japan

Accepted by the Astrophysical Journal

ABSTRACT

We estimate minimum dust abundances required for secular gravitational instability (SGI) to operate at the midplane dust layer of protoplanetary disks. For SGI to be a viable process, the growth time of the instability T_{grow} must be shorter than the radial drift time of the dust T_{drift} . The growth time depends on the turbulent diffusion parameter α , because the modes with short wavelengths are stabilized by turbulent diffusion. Assuming that turbulence is excited via the Kelvin-Helmholtz or streaming instabilities in the dust layer, and that its strength is controlled by the energy supply rate from dust accretion, we estimate the diffusion parameter and the growth time of the instability. The condition $T_{\text{grow}} < T_{\text{drift}}$ requires that the dust abundance must be greater than a critical abundance Z_{min} , which is a function of the Toomre parameter Q_g and aspect ratio h_g/r of the gas disk. For a wide range of parameter space, the required dust abundance is less than 0.1. A slight increase in dust abundance opens a possible route for the dust to directly collapse to planetesimals.

Subject headings: planets and satellites: formation — protoplanetary disks

1. INTRODUCTION

Formation processes of planetesimals have not been well understood in planet formation theory. The gravitational instability of the dust layer at the midplane of a protoplanetary disk has been proposed as a possible route to planetesimal formation. The classical scenario of gravitational instability requires high densities of dust layers to surpass the Roche limit (Goldreich & Ward 1973; Sekiya 1983). Dust sedimentation only in the vertical direction hardly achieves such a high density (Sekiya 1998). The dust layer becomes turbulent via Kelvin-Helmholtz (KH) or streaming instabilities when its dust density exceeds the gas density, which is much less than the Roche density, and further dust settling is significantly suppressed (Chiang & Youdin 2010 for review). Radial drift of the dust caused by gas drag may provide a possible route for further accumulation of the dust. When the dissipative effects of gas drag are included, the dust layer is secularly gravitationally unstable to the modes of dust accumulation in the radial direction (Ward 2000; Youdin 2005a, 2005b). This secular gravitational instability (SGI) occurs in any dust layers even if their densities are small (i.e., there is no criterion on their Toomre's Q values for SGI; Youdin 2011; Shariff & Cuzzi 2011; Michikoshi et al. 2012; these papers are referred hereafter as Y11, SC11, and MKI12, respectively).

However, the growth rate of SGI is greatly suppressed by gas drag, particularly for small particles, and could be too slow to have any effect on planetesimal formation. Y11, SC11, and MKI12 argue that the growth timescale must be shorter than the lifetime of the dust drifting toward the star owing to gas drag. The wavelength of the most unstable mode is determined by the balance between the radial accumulation of dust particles due to self-gravity and their diffusion due to gas turbulence.

Only perturbations with wavelengths sufficiently long are unstable. For stronger turbulence, wavelengths of the unstable modes, as well as growth timescales, are longer. Y11 and SC11 have calculated the growth timescales for various values of the turbulent diffusion parameter α , and have derived an upper limit on α required for the growth timescale to be shorter than the drift timescale. Their approach is general and can be applied for any disk turbulence, provided that the value of α is known.

In this paper, we focus on disk turbulence induced in the dust layer, assuming that the gas disk itself is a globally laminar flow. In such a disk, the concentration of dust particles at its midplane triggers turbulence. The velocity difference between the dust and gas induces the KH or streaming instabilities and causes turbulence in the dust layer (Chiang & Youdin 2010). The ultimate energy source for turbulence is the accretion energy of the dust drifting toward the star, regardless of the kind of instability that occurs in the dust layer. Thus, a simple energetics can be applied to estimate the turbulence strength, provided that the dust accretion velocity is known. Takeuchi et al. (2012, hereafter T12) calculate the energy supply rate to turbulence, using the classical formulae on the drift velocity of the dust (Nakagawa et al. 1986; Weidenschilling 2003; Youdin & Chiang 2004), and then estimate the turbulence strength or the value of α . T12 has shown that, from the comparison between the estimated value of α and the recent results of numerical simulations of turbulence by Johansen et al. (2006) and Bai & Stone (2010), the turbulence strength excited via KH and/or streaming instabilities can be estimated from the dust accretion rate.

While Y11, SC11, and MKI12 have derived the growth time of SGI as a function of α and other disk parameters (Equation (51) of Y11), T12 has obtained α values of turbulence in the dust layer (Equation (5) below). Combining these results gives an expression of the growth time without the unknown parameter α , as shown in Section 2.1. Consequently, in Section 2.3, the criterion for SGI

¹ taku@geo.titech.ac.jp

to operate is obtained as a condition on the dust abundance Z in the disk. For SGI to operate faster than the dust drift timescale, the dust abundance must be greater than a specific critical value Z_{\min} , which is a function of the Toomre Q value of the gas disk and the deviation fraction η of the gas velocity from the Keplerian velocity. The Z_{\min} value derived in this paper gives the minimum dust abundance required for SGI, because we consider only turbulence induced in the dust layer. If turbulence were caused by another mechanism such as magneto-rotational instability (MRI) of the gas disk, α would be larger than the value we adopted, and consequently the required value of Z_{\min} would increase. Hence, Z_{\min} derived in this paper is considered as the minimum value required for SGI in realistic disks.

2. CONDITION FOR SECULAR GRAVITATIONAL INSTABILITY

We consider a protoplanetary disk initially in a laminar flow state. Sedimentation of dust particles to the mid-plane of the disk induces turbulence via KH or streaming instabilities caused by velocity differences between the dust and gas. A (quasi)-steady dust layer forms when turbulent diffusion matches dust settling, in which steady state turbulence is maintained. We neglect intermittency of turbulence. If an extra source of turbulence is present such as global turbulence of the gas disk via MRI, the turbulence would be stronger than that excited only by the dust-gas velocity difference. Thus, in this paper, we consider the minimum strength of turbulence.

The dust particles are characterized by their stopping time t_s , which is the timescale of damping the velocity difference from the gas. We define the non-dimensional stopping time, $T_s = t_s \Omega_K$, normalized by the Keplerian frequency Ω_K . In this study, we focus on the dynamics of relatively small particles such that $T_s \lesssim 1$. Particles with $T_s \sim 1$ experience high speed collisions and the fastest radial drift, which likely hinder particle growth. SGI of the dust layer is a possible route for directly forming large bodies ($T_s \gg 1$) from small particles ($T_s \ll 1$).

In the following subsections, we compare the growth time of SGI with the orbital drift time of the dust particles due to gas drag in order to determine the condition for SGI to be a relevant process for planetesimal formation.

2.1. Timescale of Secular Gravitational Instability

In his Equation (51), Y11 shows that the growth time of SGI for small particles with $T_s \lesssim 1$, normalized by the Keplerian time Ω_K^{-1} , is

$$T_{\text{grow}} \approx \frac{\alpha Q_g^2}{Z^2 T_s^2}. \quad (1)$$

Here α is the turbulent diffusion parameter (see below), Q_g is the Toomre stability parameter of the gas disk,

$$Q_g = \frac{c_g \Omega_K}{\pi G \Sigma_g}, \quad (2)$$

where c_g is the sound speed of the gas, G is the gravitational constant, and Σ_g is the surface density of the gas disk. The disk ‘‘metallicity’’ Z is the ratio of the surface densities between the dust and gas, $Z = \Sigma_d / \Sigma_g$. The

growth time depends on the turbulent diffusion parameter α through its stabilizing effect for perturbations with short wavelengths.

Turbulence in the dust layer is induced by velocity differences between the dust and gas. If the drag force between the gas and dust were not effective, the dust would orbit with the Keplerian velocity v_K , while the gas would orbit with a sub-Keplerian velocity

$$v_g = (1 - \eta)v_K, \quad (3)$$

where $\eta = -(2\rho_g r \Omega_K^2)^{-1} \partial P / \partial r \sim (c_g / v_K)^2 \sim 10^{-3} - 10^{-2}$, ρ_g is the gas density, and P is the gas pressure. In the calculation of α , a slightly different definition of η is useful (see T12 or Appendix A in this paper). We introduce $\tilde{\eta}$ defined by

$$\tilde{\eta} = \left(\frac{v_K}{c_g} \right)^2 \eta^2 = C_\eta \eta, \quad (4)$$

where C_η is a factor of the order of unity, which depends on the radial profile of the gas disk. In this paper, we adopt $C_\eta = 1$ (i.e., $\tilde{\eta} = \eta$) for simplicity, except in Section 3 where specific disk models are considered.

T12 shows that the dust particles accrete toward the star due to gas drag and supply energy to turbulence via KH and/or streaming instabilities. Dust accretion is either caused by the gas drag acting on individual particles or by turbulent drag acting on the surface of the dust layer. The former (individual drag) is effective if the dust-to-gas ratio at the disk midplane, $f_{\text{mid}} = \rho_d / \rho_g|_{z=0}$, is less than unity, and the latter (collective drag) is effective if $f_{\text{mid}} \gtrsim 1$. Appendix A briefly summarizes dust accretion due to both drag types (see T12 for detailed discussions). The turbulence strength or the parameter α is determined by the energy supply rate from dust accretion toward the star. The approximate expression of α for $T_s \lesssim 1$ particles is given by

$$\alpha \approx \left[(C_1 C_{\text{eff}} \tilde{\eta} Z)^{-\frac{2}{3}} + (C_2 C_{\text{eff}} \tilde{\eta} Z^{-1})^{-2} \right]^{-1} T_s, \quad (5)$$

where $C_{\text{eff}} = 0.19$ is the energy supply efficiency (see T12), and $C_1 = 1.0$ and $C_2 = 1.6$ are the numerical factors. This expression connects the approximate formulae of α for the two limiting regimes of $f_{\text{mid}} \ll 1$ and $f_{\text{mid}} \gg 1$ (Equations (A2) and (A3)). Note that the condition $f_{\text{mid}} \ll 1$ (or $f_{\text{mid}} \gg 1$) corresponds to the condition $Z \ll (C_{\text{eff}} \tilde{\eta})^{1/2}$ (or $Z \gg (C_{\text{eff}} \tilde{\eta})^{1/2}$) (see Equation (A5)). The numerical factors C_1 and C_2 are adjusted to make an appropriate fit to the overall behavior of the numerical result. A comparison of this approximate expression to the numerically calculated α is shown in Appendix A. Substituting Equation (5) in Equation (1) gives

$$T_{\text{grow}} \approx \frac{Q_g^2}{Z^2 T_s} \left[(C_1 C_{\text{eff}} \tilde{\eta} Z)^{-\frac{2}{3}} + (C_2 C_{\text{eff}} \tilde{\eta} Z^{-1})^{-2} \right]^{-1}, \quad (6)$$

showing that T_{grow} is a function of the disk parameters ($\tilde{\eta}$, Z , Q_g) and is inversely proportional to T_s .

2.2. Timescale of Radial Drift

According to T12, the non-dimensional timescale of the radial drift of dust particles due to gas drag is estimated

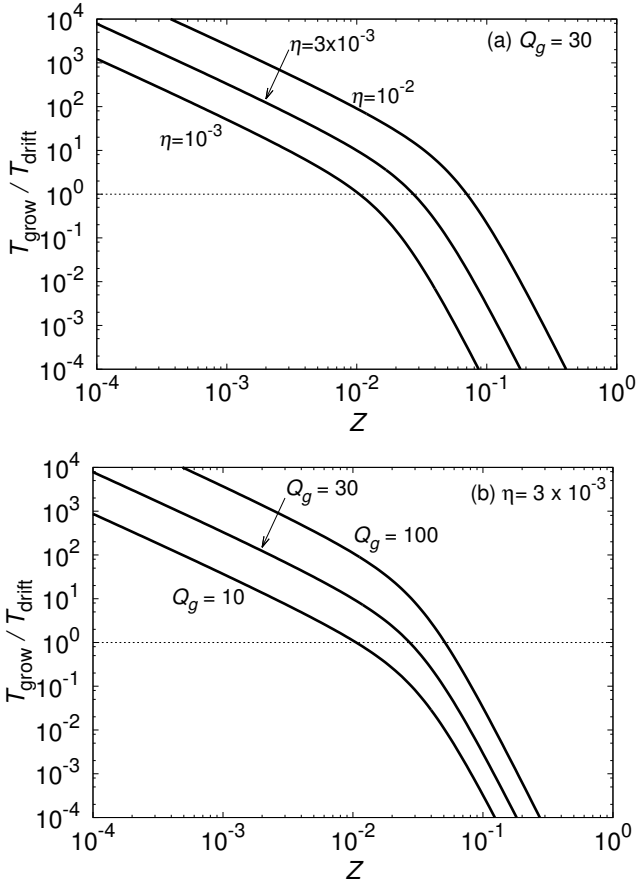


FIG. 1.— Ratio of the growth time to the radial drift time, $T_{\text{grow}}/T_{\text{drift}}$, against dust abundance Z . (a) For models with a fixed Toomre parameter of the gas disk, $Q_g = 30$. (b) For models with a fixed deviation fraction of the gas velocity from the Keplerian velocity, $\eta = 3 \times 10^{-3}$. The horizontal dotted line indicates $T_{\text{grow}} = T_{\text{drift}}$.

as

$$T_{\text{drift}} \approx \frac{f_{\text{mid}} + 1}{2\eta T_s}, \quad (7)$$

where the midplane dust-to-gas ratio f_{mid} is approximately given by

$$f_{\text{mid}} \approx \left(\frac{Z^2}{C_1 C_{\text{eff}} \tilde{\eta}} \right)^{\frac{1}{3}} + \left(\frac{Z^2}{C_2 C_{\text{eff}} \tilde{\eta}} \right). \quad (8)$$

In the above estimate, both individual and collective drags are considered. Derivation of the above expressions are described in Appendix A. The timescale of the radial drift is a function of $(\tilde{\eta}, Z)$ and is inversely proportional to T_s .

2.3. Comparison of Timescales

2.3.1. Minimum Dust Abundances

Y11, SC11, and MKI12 show that dust layers are always unstable and subject to SGI, but the growth rate for particles tightly coupled to the gas is strongly suppressed by gas drag. The growth timescale can be larger than the other timescales, in which the dust layer evolves significantly by other processes such as the dispersal of the gas disk and the radial drift of the dust to the star. The condition for SGI to be a relevant process for planetesimal formation dictates that its growth timescale must be

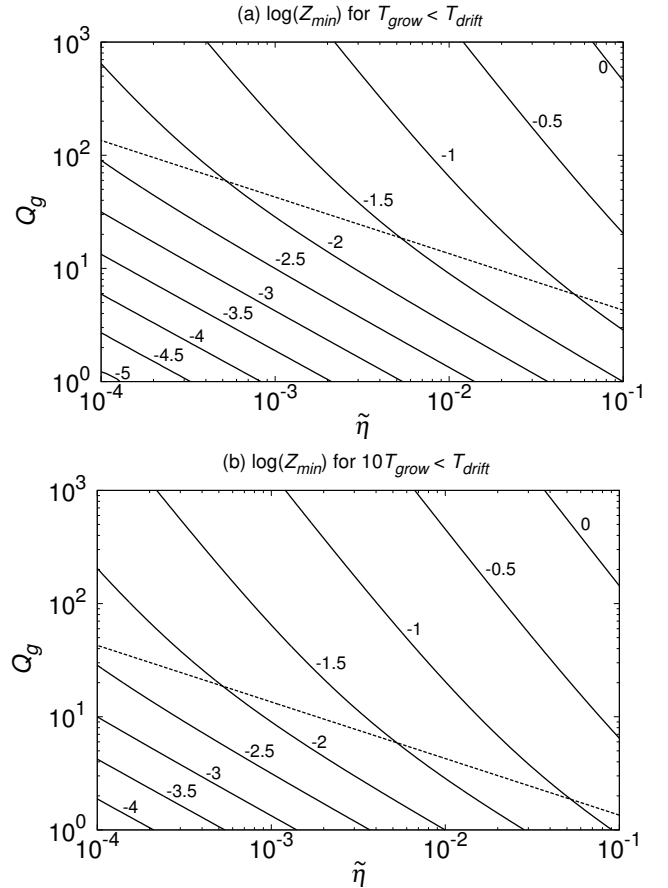


FIG. 2.— Contour map of the minimum dust abundance Z_{min} on the $\tilde{\eta}$ - Q_g plane. (a) Z_{min} required for the condition $T_{\text{grow}} < T_{\text{drift}}$. The contours are labeled by $\log(Z_{\text{min}})$. The dashed line shows the locus of $Z_{\text{min}} = (C_{\text{eff}}\tilde{\eta})^{1/2}$ (i.e., $f_{\text{mid}} \approx 1$ when $Z = Z_{\text{min}}$). (b) Z_{min} required for the condition $10T_{\text{grow}} < T_{\text{drift}}$.

shorter than the other evolution timescales. Y11 shows that the radial drift imposes the most stringent condition for a wide range of disk parameters. We discuss the condition for $T_{\text{grow}} < T_{\text{drift}}$. Because both T_{grow} and T_{drift} are inversely proportional to T_s , the ratio $T_{\text{grow}}/T_{\text{drift}}$ is independent of T_s ; that is, the condition $T_{\text{grow}} < T_{\text{drift}}$ is not affected by particle size. We consider dependence of $T_{\text{grow}}/T_{\text{drift}}$ on the parameters $(\tilde{\eta}, Z, Q_g)$.

First, we examine the limiting cases of $Z \ll (C_{\text{eff}}\tilde{\eta})^{1/2}$ and $Z \gg (C_{\text{eff}}\tilde{\eta})^{1/2}$ ($f_{\text{mid}} \ll 1$ and $f_{\text{mid}} \gg 1$). In both limits,

$$\frac{T_{\text{grow}}}{T_{\text{drift}}} \approx \begin{cases} 2C_{\eta}^{-1} (C_1 C_{\text{eff}})^{2/3} \tilde{\eta}^{5/3} Q_g^2 Z^{-4/3} & \text{for } Z \ll (C_{\text{eff}}\tilde{\eta})^{1/2} \\ 2C_{\eta}^{-1} (C_2 C_{\text{eff}})^3 \tilde{\eta}^4 Q_g^2 Z^{-6} & \text{for } Z \gg (C_{\text{eff}}\tilde{\eta})^{1/2} \end{cases}. \quad (9)$$

For $Z \ll (C_{\text{eff}}\tilde{\eta})^{1/2}$, $T_{\text{grow}}/T_{\text{drift}}$ is proportional to $Z^{-4/3}$, while for $Z \gg (C_{\text{eff}}\tilde{\eta})^{1/2}$ it rapidly decreases as $T_{\text{grow}}/T_{\text{drift}} \propto Z^{-6}$. In Figure 1, $T_{\text{grow}}/T_{\text{drift}}$ is plotted against Z for various values of $\tilde{\eta}$ and Q_g . For $Z \gg (C_{\text{eff}}\tilde{\eta})^{1/2} \sim 10^{-2}$, it is evident that $T_{\text{grow}}/T_{\text{drift}}$ rapidly decreases. For sufficiently large values of Z , $T_{\text{grow}}/T_{\text{drift}}$ is less than unity, indicating that SGI oper-

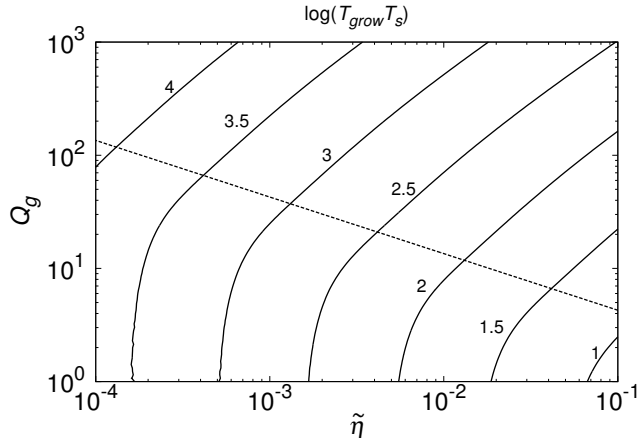


FIG. 3.— Contour map of the growth time multiplied by the stopping time, $T_{\text{grow}}T_s$, on the $\tilde{\eta}$ - Q_g plane. The contours are labeled by $\log(T_{\text{grow}}T_s)$. In calculating $T_{\text{grow}}(\tilde{\eta}, Q_g)$, the minimum dust abundances $Z_{\text{min}}(\tilde{\eta}, Q_g)$ are used. The dashed line shows the locus of $Z_{\text{min}} = (C_{\text{eff}}\tilde{\eta})^{1/2}$.

ates faster than the radial drift of the dust. From Figure 1, the minimum dust abundance required for SGI, Z_{min} , is determined as Z satisfying $T_{\text{grow}}/T_{\text{drift}} = 1$. The minimum dust abundance Z_{min} ranges between 10^{-2} and 10^{-1} for parameters $(\tilde{\eta}, Q_g)$ adopted in Figure 1.

In Figure 2(a), the minimum dust abundance Z_{min} required for $T_{\text{grow}} < T_{\text{drift}}$ is plotted as contours on the $\tilde{\eta}$ - Q_g plane. The locus of $Z_{\text{min}} = (C_{\text{eff}}\tilde{\eta})^{1/2}$ is represented as a dashed line on the $\tilde{\eta}$ - Q_g plane. On this line, the midplane dust-to-gas ratio f_{mid} becomes close to unity when $Z = Z_{\text{min}}$. Substitution of $Z = (C_{\text{eff}}\tilde{\eta})^{1/2}$ into Equation (9) shows that the condition $T_{\text{grow}}/T_{\text{drift}} = 1$ (i.e., $Z = Z_{\text{min}}$) becomes $Q_g \approx \tilde{\eta}^{-1/2}$. Thus, the dashed line in Figure 2(a) is linear with a slope of $-1/2$. Above this line, $Z_{\text{min}} > (C_{\text{eff}}\tilde{\eta})^{1/2}$ (and $f_{\text{mid}} > 1$ for $Z = Z_{\text{min}}$); below it, $Z_{\text{min}} < (C_{\text{eff}}\tilde{\eta})^{1/2}$ (and $f_{\text{mid}} < 1$). The dependence of Z_{min} on $(\tilde{\eta}, Q_g)$ is expressed as

$$Z_{\text{min}} \approx \begin{cases} (8C_{\eta}^{-3}C_1^2C_{\text{eff}}^2\tilde{\eta}^5Q_g^6)^{1/4} & \text{for } Q_g \ll \tilde{\eta}^{-1/2} \\ (2C_{\eta}^{-1}C_2^3C_{\text{eff}}^3\tilde{\eta}^4Q_g^2)^{1/6} & \text{for } Q_g \gg \tilde{\eta}^{-1/2} \end{cases} \quad (10)$$

Larger dust abundances are required for larger $\tilde{\eta}$ (i.e., hotter gas disks) and larger Q_g (i.e., less massive gas disks). In standard models for protoplanetary disks, $\tilde{\eta} = 10^{-3} - 10^{-2}$, and $Q_g = 10 - 1000$ (see Figure 6 below). Thus, if the dust abundance Z is larger than 0.1, such dusty disks operate SGI. If the gas disk is so cold that $\tilde{\eta}$ is as small as 10^{-3} and if it is so massive that Q_g is as small as 10, then even a standard value $Z = 0.01$ is sufficiently large to operate SGI.

2.3.2. Dependence of Z_{min} on Some Model Parameters

The growth time T_{grow} is just a time for density perturbations to increase e -fold. Because many e -folds are needed for a significant density increase, actual condition for SGI would be $RT_{\text{grow}} < T_{\text{drift}}$, where $R > 1$ is the required number of e -folding. From Equation (9) the minimum dust abundance Z_{min} scales as $Z_{\text{min}} \propto R^{3/4}$ for $Q_g \ll (R\tilde{\eta})^{-1/2}$ and $Z_{\text{min}} \propto R^{1/6}$ for $Q_g \gg (R\tilde{\eta})^{-1/2}$. Figure 2(b) shows Z_{min} derived for the condition $10T_{\text{grow}} < T_{\text{drift}}$. For less massive gas

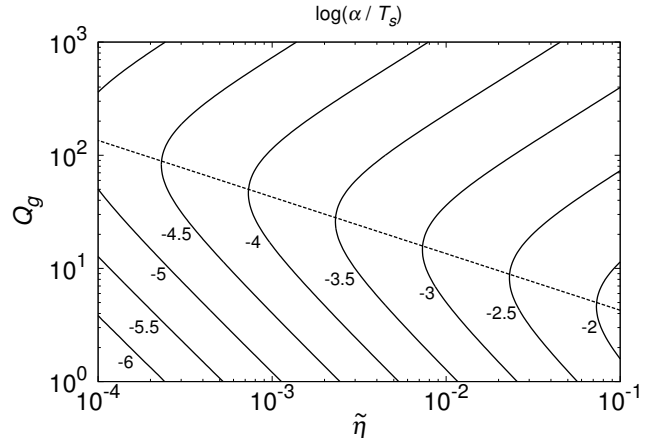


FIG. 4.— Contour map of the diffusion parameter divided by the stopping time, α/T_s , on the $\tilde{\eta}$ - Q_g plane for the dust layer with Z_{min} . The contours are labeled by $\log(\alpha/T_s)$. The dashed line shows the locus of $Z_{\text{min}} = (C_{\text{eff}}\tilde{\eta})^{1/2}$.

disks ($Q_g \gg (R\tilde{\eta})^{-1/2}$; above the dashed line in Figure 2), Z_{min} depends only weakly on R . For massive gas disks ($Q_g \ll (R\tilde{\eta})^{-1/2}$), required Z_{min} is higher for larger R ($Z_{\text{min}} \propto R^{3/4}$), but would not be too high (i.e., $Z_{\text{min}} \lesssim 0.1$ even for $R = 10$; see the region below the dashed line in Figure 2(b)). In the following discussions, we use the condition $T_{\text{grow}} < T_{\text{drift}}$.

In this paper, it is assumed that about 20% of the dust accretion energy is used for turbulence excitation ($C_{\text{eff}} = 0.19$). This value is determined by comparison with the numerical simulations of turbulence excited via KH instability by Johansen et al. (2006). Because their simulation was two-dimensional, the realistic value of C_{eff} could be different. For example, three-dimensional simulations by Lee et al. (2010) show that the critical Richardson number for KH instability increases with Z , implying that C_{eff} also increases with Z (see discussion in Section 5.2.1 of T12). As shown in Equation (10), $Z_{\text{min}} \propto C_{\text{eff}}^{1/2}$. For the maximum efficiency ($C_{\text{eff}} = 1$), Z_{min} would be about 2 times larger than our estimate.

2.4. Conditions on T_{grow} , α , and λ

In the previous subsection, the condition for $T_{\text{grow}} < T_{\text{drift}}$ was discussed. Next, we discuss other constraints required for SGI operation. First, we consider the condition for the growth time to be less than the disk life time. The growth time multiplied by the stopping time, $T_{\text{grow}}T_s$, is plotted on the $\tilde{\eta}$ - Q_g plane in Figure 3. The values of $T_{\text{grow}}(\tilde{\eta}, Q_g)$ are calculated using the minimum dust abundance $Z = Z_{\text{min}}(\tilde{\eta}, Q_g)$, the values of which differ according to $(\tilde{\eta}, Q_g)$ as shown in Figure 2. For larger values of Z , T_{grow} is shorter ($T_{\text{grow}} \propto Z^{-4/3}$ for $Z < (C_{\text{eff}}\tilde{\eta})^{1/2}$ and $T_{\text{grow}} \propto Z^{-4}$ for $Z > (C_{\text{eff}}\tilde{\eta})^{1/2}$). Because T_{grow} is inversely proportional to T_s , the contours are labeled by $\log(T_{\text{grow}}T_s)$. Thus, the growth timescale is obtained by dividing the value in Figure 3 by T_s . For $\tilde{\eta} > 10^{-3}$ and $Q_g < 10^2$, T_{grow} is less than $10^3T_s^{-1}\Omega_{\text{K}}^{-1}$. Thus at 1AU, the dust layer composed of $T_s \gtrsim 10^{-3}$ particles (size $a \gtrsim 1\text{mm}$) with the dust abundance Z_{min} operates SGI within a disk life time of $\sim 1\text{Myr}$.

Figure 4 shows the diffusion parameter α due to turbulence induced in the dust layer with the abundance

Z_{\min} . Because α is proportional to T_s , the contours are labeled by $\log(\alpha/T_s)$. Thus, the α value is obtained by multiplying the value in Figure 4 by T_s . For $\tilde{\eta} > 10^{-3}$ and $Q_g < 10^2$, α is larger than $10^{-4}T_s$, except for very small $Q_g \lesssim 10$ and $\tilde{\eta} \lesssim 3 \times 10^{-3}$. If the disk is turbulent due to other mechanisms than that originating from the dust layer and if turbulent diffusion is stronger than that shown in Figure 4, then the required value for Z would be higher. Even in the dead zone where MRI is not active, the gas could have turbulent motion, causing diffusion of the dust (Fleming & Stone 2003). Okuzumi & Hirose (2011) show that lower values of the diffusion coefficient in the dead zone are realized for a wider dead zone or weaker vertical magnetic fields. For example, if the plasma β (the ratio of gas pressure to magnetic pressure) is greater than 3×10^6 , the diffusion coefficient due to MRI turbulence is less than 10^{-5} (see model X1b of Okuzumi & Hirose 2011). In such a weakly magnetized disk and for $T_s > 0.1$ particles, turbulence originating in the dust layer is stronger than MRI turbulence in the dead zone.

The wavelength of the most unstable mode must be smaller than the disk radius. The wavelength λ is given in Equation (56) of Y11. The ratio of λ to half of the disk radius r is

$$\frac{2\lambda}{r} \approx \frac{4\pi\alpha Q_g \tilde{\eta}^{1/2}}{C_\eta Z T_s}, \quad (11)$$

and is plotted in Figure 5 for disks with the minimum dust abundances Z_{\min} . Note that $2\lambda/r$ does not depend on T_s , because α is proportional to T_s . Figure 5 shows that λ is smaller than $r/2$ if $\tilde{\eta}$ is less than 3×10^{-2} , although it is still comparable to $r/2$ even for $\tilde{\eta}$ as small as 3×10^{-3} . In the analysis by Y11, SC11, and MKI12, the gas disk is assumed to behave as a stationary background, and its velocity profiles are not affected by the gravity of the dust layer. However, the response of the gas to perturbations longer than the gas scale height is not clear. For perturbations with smaller wavelengths to be unstable, larger values of Z than those shown in Figure 2 are required. The wavelength varies as $\lambda \propto Z^{-1/3}$ for $Z < (C_{\text{eff}}\tilde{\eta})^{1/2}$ and $\lambda \propto Z^{-3}$ for $Z > (C_{\text{eff}}\tilde{\eta})^{1/2}$. In the latter regime ($Z > (C_{\text{eff}}\tilde{\eta})^{1/2}$), an increase by a factor of 2 in Z results in an order of magnitude decrease in λ , while in the former regime, reduction in the wavelength requires a large increase in Z .

3. MINIMUM DUST ABUNDANCES FOR VARIOUS DISK MODELS

In the previous section, minimum dust abundances for SGI were obtained for given parameters $(\tilde{\eta}, Q_g)$. In this section, we consider several disk models. We adopt power-law profiles for density and temperature distributions of the gas disk, such that

$$\Sigma_g = \Sigma_{g,0} r_{\text{AU}}^{-p}, \quad (12)$$

$$T = T_0 r_{\text{AU}}^{-q}, \quad (13)$$

where r_{AU} is the distance from the star measured in AU. In such a disk, $Q_g \propto r_{\text{AU}}^{(2p-q-3)/2}$ and $\tilde{\eta} \propto r_{\text{AU}}^{1-q}$. We consider two cases of hot and cold gas disks, $T_0 = 300\text{K}$ and 150K , while we fix the power-law index $q = 1/2$.

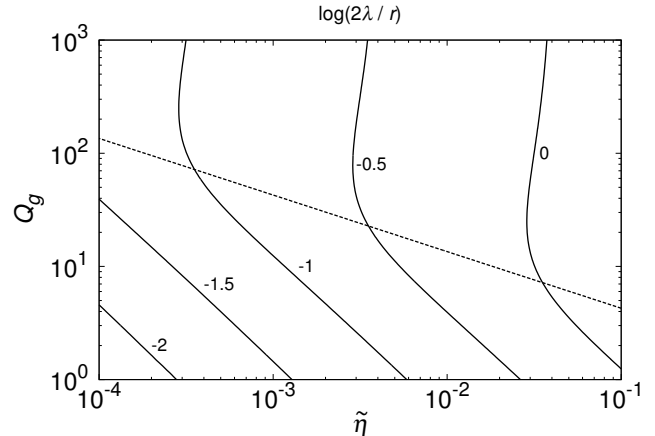


FIG. 5.— Contour map of the normalized wavelength of the most unstable mode $2\lambda/r$ on the $\tilde{\eta}$ - Q_g plane for the dust layer with Z_{\min} . The contours are labeled by $\log(2\lambda/r)$. The dashed line shows the locus of $Z_{\min} = (C_{\text{eff}}\tilde{\eta})^{1/2}$.

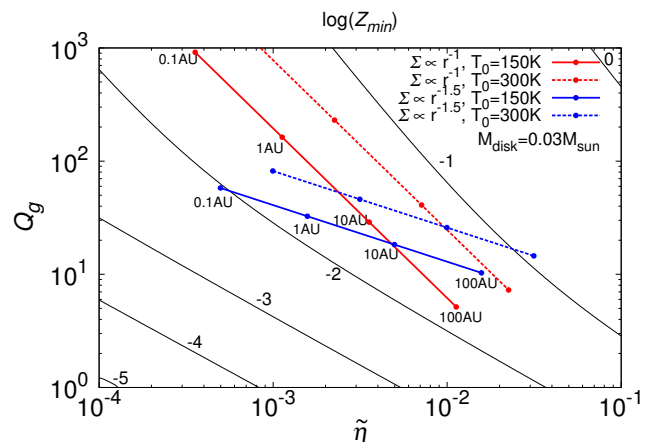


FIG. 6.— Models of the gas disks are plotted on the $\tilde{\eta}$ - Q_g plane. Red and blue lines represent models with shallow and steep density profiles, $\Sigma \propto r^{-1}$ and $\Sigma \propto r^{-1.5}$, respectively. Solid and dashed lines indicate models of cold and hot gas disks, $T_0 = 150\text{K}$ and $T_0 = 300\text{K}$, respectively. Dots on the lines show locations on the disks, 0.1, 1, 10, and 100 AU. The disk mass is $M_{\text{disk}} = 0.03M_\odot$. Contours show $\log(Z_{\min})$.

For the density profile, $p = 1.0$ and 1.5 are adopted and the mass of the gas disk inside 100 AU is varied within $M_{\text{disk}} = 10^{-2} - 10^{-1}M_\odot$. Figure 6 shows the variability in the values of $\tilde{\eta}$ and Q_g between the models and with r . In this figure, models with $M_{\text{disk}} = 3 \times 10^{-2}M_\odot$ are shown. For various values of M_{disk} , Q_g scales as $Q_g \propto M_{\text{disk}}$.

Figure 7 shows the required minimum dust abundances Z_{\min} against r_{AU} for various disk models. For the steep density profile ($p = 1.5$; blue dashed lines), $Z_{\min} \propto r_{\text{AU}}^{1/4}$. (In the regime of $Q_g \ll \tilde{\eta}^{-1/2}$ of Equation (10), $Z_{\min} \propto \tilde{\eta}^{5/4} Q_g^{3/2} \propto r_{\text{AU}}^{1/4}$; in the $Q_g \gg \tilde{\eta}^{-1/2}$ regime, $Z_{\min} \propto \tilde{\eta}^{2/3} Q_g^{1/3} \propto r_{\text{AU}}^{1/4}$). SGI is more viable at the inner part of the disk. For $p = 1.0$ (red solid lines), $Z_{\min} \propto r_{\text{AU}}^{1/12}$ only weakly depends on r (in the $Q_g \gg \tilde{\eta}^{-1/2}$ regime). The outer part of the disk with $M_{\text{disk}} = 10^{-1}M_\odot$ and $p = -1$ is in the $Q_g \ll \tilde{\eta}^{-1/2}$ regime, and Z_{\min} decreases as $Z_{\min} \propto r^{-1/2}$. Even in

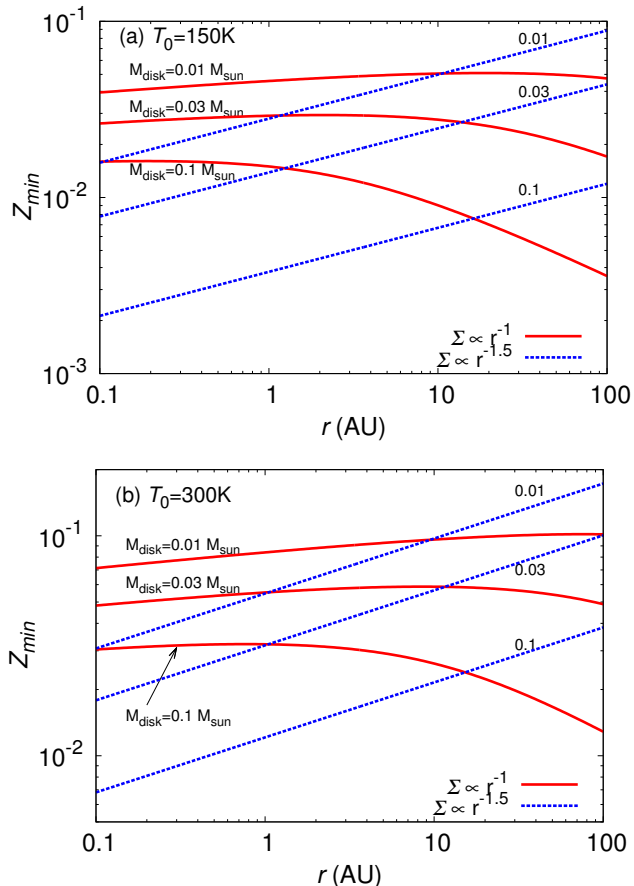


FIG. 7.— Minimum dust abundances Z_{\min} for various disk models. (a) Cold disks ($T_0 = 150\text{K}$). (b) Hot disks ($T_0 = 300\text{K}$). Red solid and blue dashed lines represent models with shallow and steep density profiles, $\Sigma_g \propto r^{-1}$ and $\Sigma_g \propto r^{-1.5}$, respectively.

the hot gas disks ($T_0 = 300\text{K}$) with a mass as small as $M_{\text{disk}} = 10^{-2}M_{\odot}$, the required dust abundances for SGI are less than 0.1. If the temperature at the disk midplane is as cold as $T_0 \approx 150\text{K}$, as expected in passive disks that are heated only by stellar radiation (Chiang & Goldreich 1997; Tanaka et al. 2005), SGI operates for $Z_{\min} < 0.05$ at 10AU of disks with $M_{\text{disk}} = 10^{-2}M_{\odot}$.

4. DISCUSSION

Analysis in this paper assumes that turbulence is induced in the dust layer. If the dust abundance at the midplane f_{mid} is larger than unity ($Z \gtrsim (C_{\text{eff}}\tilde{\eta})^{1/2}$), turbulence weakens with increasing Z as $\alpha \propto Z^{-2}$ (Equation (5)). The growth timescale of SGI rapidly decreases as $T_{\text{grow}} \propto Z^{-4}$ (Equation (6)). A slight increase in Z makes SGI viable. Y11 also estimated the minimum dust abundance Z_{η} required for SGI (Equation (69) of Y11), assuming that the turbulent diffusion parameter of a dense dust layer ($f_{\text{mid}} \gtrsim 1$) was $\alpha_{\eta} \approx T_s \tilde{\eta}$ (Equation (68) of Y11), independent of Z . This estimate for α_{η} adopted by Y11 corresponds to the maximum value of $\alpha(Z)$ at $Z \approx (C_{\text{eff}}\tilde{\eta})^{1/2}$ in our estimate (Equation (5)). If α had a constant value α_{η} for all Z , the condition $T_{\text{grow}} < T_{\text{drift}}$ would be

$$Z > Z_{\eta} \sim \eta^{5/6} Q_g^{2/3}, \quad (14)$$

where we used $f_{\text{mid}} = Zh_g/h_d$ and $h_d/h_g \sim \eta^{1/2}$. Note that this Equation (14) differs from Equation (69) of Y11, because we use Equation (7), in which $T_{\text{drift}} \propto f_{\text{mid}}$, while Y11 assumes $T_{\text{drift}} \propto f_{\text{mid}}^2$ (see discussion following Equation (A6) below). As discussed in T12, accumulation of the dust increases the inertia of the dust layer and decelerates the inward drift of the dust, resulting in weaker turbulence. Considering $\alpha \propto Z^{-2}$, the condition $T_{\text{grow}} < T_{\text{drift}}$ becomes

$$Z > Z_{\min} \sim \eta^{2/3} Q_g^{1/3}, \quad (15)$$

as shown in Equation (10). We ignore numerical coefficients such as C_{eff} and C_{η} . These two conditions (Equations (14) and (15)) coincide when $f_{\text{mid}} = 1$ (i.e., $Z_{\eta} = Z_{\min} \approx \eta^{1/2}$) or when $Q_g = Q_{g,0}(\eta) \equiv \eta^{-1/2}$ (i.e., on the dashed line in Figures 2-5). If the disk's Q_g is greater than $Q_{g,0}$, then the latter condition (Equation (15)) permits smaller dust abundances for SGI by a factor of $Z_{\min}/Z_{\eta} = (Q_g/Q_{g,0})^{-1/3}$. For example, at 1AU on a disk with $M_{\text{disk}} = 0.03M_{\odot}$, $\Sigma_g \propto r^{-1}$, and $T_0 = 300\text{K}$, Equation (15) gives $Z_{\min} = 0.11$, which is smaller by a factor of 2 than the value $Z_{\eta} = 0.23$ predicted by Equation (14). Considering the Z dependence of α reduces the required minimum value Z_{\min} for SGI as compared with that derived by Y11.

5. SUMMARY

We analyze the condition for SGI occurrence in the dust layer. The growth timescale of the instability must be shorter than the radial drift timescale of the dust. The growth timescale decreases as turbulence weakens. The necessary condition for SGI is obtained by considering turbulence induced in the dust layer. Using the turbulence strength estimated from the energy supply rate from the accreting dust, the minimum dust abundances for SGI, Z_{\min} , are derived as a function of the Toomre Q_g parameter of the gas disk and the deviation fraction η of the gas velocity from the Keplerian value. If the dust particles are small and their stopping time is less than the Keplerian time ($T_s < 1$), Z_{\min} is independent of T_s . For disks with $Q_g \sim 10^2$ and $\eta \sim 10^{-2}$, SGI occurs if $Z \gtrsim 0.1$. The required Z decreases with decreasing Q_g and η , becoming as small as 0.01 for $Q_g \sim 10$ and $\eta \sim 10^{-3}$. Such an increase in Z from the solar abundance is expected to occur through several processes, including the radial drift of the dust and dispersal of the gas from the disk (Youdin & Shu 2002; Takeuchi & Lin 2002; Takeuchi et al. 2005). Therefore, SGI provides a possible route for small particles to directly collapse to planetesimals in an initially laminar disk. If the gas disk were globally turbulent via MRI, for example, the required Z would be larger than Z_{\min} estimated in this paper.

We thank Takayuki Muto, Satoshi Okuzumi, Hidekazu Tanaka, Shugo Michikoshi, and Naoki Ishitsu for useful discussions. We also thank an anonymous referee for helpful comments. This work was supported by Grants-in-Aid for Scientific Research, Nos. 20244013 and 20540232 from the Ministry of Education, Culture, Sports, Science, and Technology, Japan.

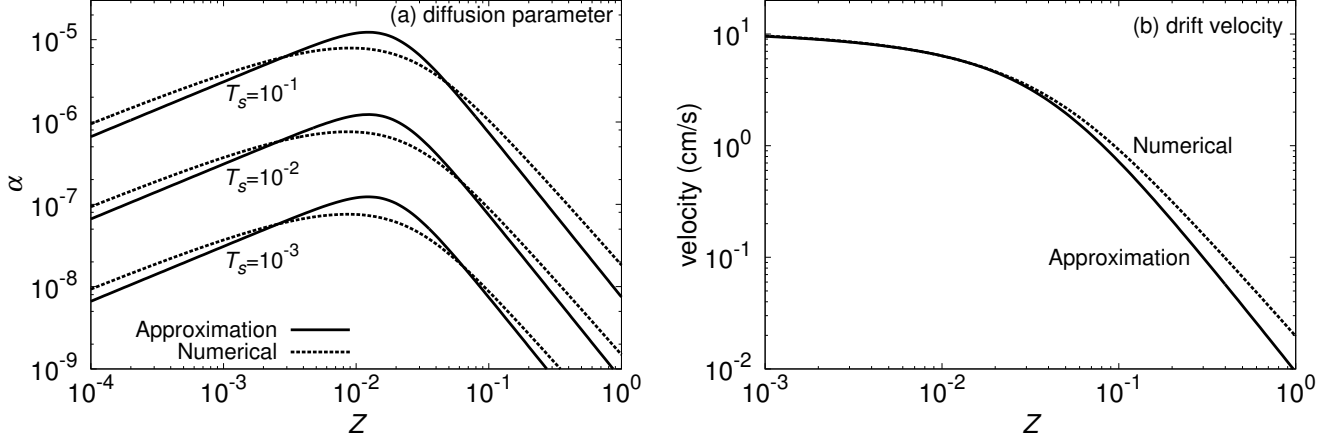


FIG. 8.— Comparison of approximate expressions with numerical results for (a) turbulent diffusion parameter α and (b) dust radial drift velocity $v_{d,r}$. Solid lines represent approximate expressions (A4) and (A6), and dashed lines are numerically calculated by T12. (a) Diffusion parameter α is plotted for $T_s = 10^{-3}, 10^{-2}$, and 10^{-1} . (b) Radial drift velocity $v_{d,r}$ is plotted for $T_s = 10^{-3}$.

APPENDIX

APPROXIMATE EXPRESSIONS OF DIFFUSION PARAMETER AND RADIAL DRIFT RATE

In this Appendix, we evaluate an approximate expression of the turbulent diffusion parameter α for small particle limit ($T_s \ll 1$) according to T12. We consider turbulence excited via KH or streaming instabilities of the dust layer. The strength of the turbulence is controlled by the dust accretion rate. The dust particles accrete toward the star either due to the gas drag on individual particles (Nakagawa et al. 1986) or collective drag exerted on the entire dust layer (Weidenschilling 2003; Youdin & Chiang 2004). Individual drag dominates if the dust-to-gas ratio in the dust layer is less than unity ($f_{\text{mid}} \lesssim 1$), while collective drag is important if $f_{\text{mid}} \gtrsim 1$.

First, we consider individual drag (for $f_{\text{mid}} \lesssim 1$). Using the formula derived by Nakagawa et al. (1986; or Equation (9) of T12, hereafter Equation (T9)), the accretion velocity of small dust particles ($T_s \lesssim 1$) is

$$v_{d,r} = -2T_s \eta v_K. \quad (\text{A1})$$

To satisfy angular momentum conservation, the gas moves outward with the velocity $v_{g,r} = -v_{d,r} \rho_d / \rho_g$, where ρ_d (ρ_g) is the dust (gas) density. The effective gravities (including the pressure gradient force) acting on the dust and gas are $g_d = -r \Omega_K^2$ and $g_g = -(1 - 2\eta)r \Omega_K^2$, respectively. The net work done by these effective gravities on a unit surface area of the dust layer is calculated as $\Delta E_{\text{drag}} \sim \int (\rho_d g_d v_{d,r} + \rho_g g_g v_{g,r}) dz \sim \eta^2 v_K^2 \Omega_K T_s \Sigma_d$ (Equation (T12)). The energy dissipation due to turbulence is estimated as $\Delta E_{\text{turb}} \sim \Sigma_{\text{layer}} u_{\text{eddy}}^2 / \tau_{\text{eddy}}$, where Σ_{layer} is the surface density of the dust layer, and u_{eddy} and τ_{eddy} are the typical values for the velocity and turnover time of the largest eddies, respectively. Adopting the so-called “ α prescription”, we evaluate $u_{\text{eddy}} \sim \sqrt{\alpha c_g}$ and $\tau_{\text{eddy}} \sim \Omega_K^{-1}$ (Cuzzi et al. 2001). For $f_{\text{mid}} \lesssim 1$, the column density of the dust layer is dominated by the gas, and thus $\Sigma_{\text{layer}} \sim \Sigma_g h_d / h_g$. Here, h_d / h_g is the ratio of the scale heights of the dust layer and gas disk, and is given by $h_d / h_g \approx \sqrt{\alpha / T_s}$ (Equation (T4)). Then, the energy dissipation rate is $\Delta E_{\text{turb}} \sim \sqrt{\alpha^3 / T_s} h_g^2 \Omega_K^3 \Sigma_g$. Equating the energy supply and dissipation rates of turbulence, with an efficiency parameter for the energy supply, $\Delta E_{\text{turb}} \sim C_{\text{eff}} \Delta E_{\text{drag}}$, gives

$$\alpha \sim (C_{\text{eff}} \tilde{\eta} Z)^{2/3} T_s. \quad (\text{A2})$$

The collective drag force in the θ -direction on a unit surface area is estimated by the plate drag approximation for $f_{\text{mid}} \gtrsim 1$ as $P_{\theta z} \sim \rho_g \nu \partial v_{g,\theta} / \partial z \sim -\rho_g \nu \eta v_K / h_d$, where ν is the turbulent viscosity, and the velocity shear in the vertical direction $\partial v_{g,\theta} / \partial z$ is estimated as $\eta v_K / h_d$. This drag causes accretion of the dust layer and an outward motion of the upper gas layer. The dust layer loses energy $\Omega_K r P_{\theta z}$ and the upper gas layer gains energy $(1 - \eta) \Omega_K r P_{\theta z}$, where the work done by gas pressure is taken into account. The net energy liberation rate is $\Delta E_{\text{vis}} \sim -\eta \Omega_K r P_{\theta z} \sim \eta^2 v_K^2 \Omega_K T_s \Sigma_d / f_{\text{mid}}$ (Equation (T18)), where we used $\nu \sim h_d^2 T_s \Omega_K$ and $h_d = h_g \Sigma_d / (\Sigma_g f_{\text{mid}})$ (Equations (T16) and (T6)). The energy dissipation rate is $\Delta E_{\text{turb}} \sim \Sigma_{\text{layer}} u_{\text{eddy}}^2 / \tau_{\text{eddy}} \sim \alpha h_g^2 \Omega_K^3 \Sigma_d$, where $\Sigma_{\text{layer}} \sim \Sigma_d$ is dominated by the dust. Equating $\Delta E_{\text{turb}} \sim C_{\text{eff}} \Delta E_{\text{vis}}$ gives

$$\alpha \sim (C_{\text{eff}} \tilde{\eta} Z^{-1})^2 T_s, \quad (\text{A3})$$

where we use $f_{\text{mid}} \approx Z \sqrt{T_s / \alpha}$ (Equation (T6)). Expressions (A2) and (A3) are the same as Equation (T28), except for numerical factors and the adoption of a slightly steeper power-law index ($\delta = 1$ in Equation (A3) instead of $\delta = 0.94$ in Equation (T28)) to simplify analytical expressions. Connecting these expressions gives

$$\alpha \approx \left[(C_1 C_{\text{eff}} \tilde{\eta} Z)^{-\frac{2}{3}} + (C_2 C_{\text{eff}} \tilde{\eta} Z^{-1})^{-2} \right]^{-1} T_s, \quad (\text{A4})$$

where the numerical factors $C_1 = 1.0$ and $C_2 = 1.6$ are set to fit the numerical result of T12. In Figure 8(a), the approximate expression (A4) is compared to the numerical result of T12. The approximation overestimates α around $Z = \sqrt{C_{\text{eff}}\tilde{\eta}}$ and underestimates it for large Z . However, the error is less than 2 for $10^{-4} < Z < 10^{-1}$, and the overall behavior appears to be acceptable.

The midplane dust-to-gas ratio $f_{\text{mid}} = Zh_g/h_d \approx Z\sqrt{T_s/\alpha}$ is, from Equations (A2) and (A3), $f_{\text{mid}} \sim [Z^2/(C_{\text{eff}}\tilde{\eta})]^{1/3}$ for $f_{\text{mid}} \lesssim 1$, and $f_{\text{mid}} \sim Z^2/(C_{\text{eff}}\tilde{\eta})$ for $f_{\text{mid}} \gtrsim 1$. Connecting these two expressions gives an approximate formula for f_{mid} as

$$f_{\text{mid}} \approx \left(\frac{Z^2}{C_1 C_{\text{eff}} \tilde{\eta}} \right)^{\frac{1}{3}} + \left(\frac{Z^2}{C_2 C_{\text{eff}} \tilde{\eta}} \right). \quad (\text{A5})$$

From the above Equation (A5), it is seen that $f_{\text{mid}} \approx 1$ when $Z \approx (C_{\text{eff}}\tilde{\eta})^{1/2}$.

The drift velocity of the dust in the limit of $f_{\text{mid}} \ll 1$ and $T_s \ll 1$ is given in Equation (A1). In the limit of $f_{\text{mid}} \gg 1$, $v_{d,r} \sim rP_{\theta z}/(v_K \Sigma_d) \sim \eta v_K T_s / f_{\text{mid}}$ (Equation (T51)). Connecting these limits, we estimate

$$v_{d,r} \approx -\frac{2T_s \eta v_K}{f_{\text{mid}} + 1}, \quad (\text{A6})$$

which gives the dust drift timescale given in Equation (7). This approximate expression is compared with the numerical calculation by T12 in Figure 8(b), which shows that the above expression provides a good approximation. Note that $v_{d,r} \propto f_{\text{mid}}^{-1}$ for $f_{\text{mid}} \gg 1$. Equation (2.11) of Nakagawa et al. (1986) shows that, due to individual drag, the radial velocity of the dust particles at the midplane is proportional to f_{mid}^{-2} . However, the average velocity of the dust layer, $\int \rho_d v_{d,r} dz / \Sigma_d$, is approximately proportional to f_{mid}^{-1} , provided that the dust density profile $\rho_d(z)$ is Gaussian. The drift velocity due to collective drag is also proportional to f_{mid}^{-1} , as shown in Equation (A6). Thus, for $f_{\text{mid}} > 1$, the radial drift time derived from the particle velocity at the midplane ($T_{\text{drift}} \propto f_{\text{mid}}^2$), which is adopted in Y11, SC11, and MKI12, overestimates the average drift time ($T_{\text{drift}} \propto f_{\text{mid}}$), resulting in a less strict condition for $T_{\text{grow}} < T_{\text{drift}}$ than reality.

REFERENCES

- Bai, X.-N., & Stone, J. M. 2010, *ApJ*, 722, 1437
Chiang, E. I., & Goldreich, P. 1997, *ApJ*, 490, 368
Chiang, E., & Youdin, A. N. 2010, *Annual Review of Earth and Planetary Sciences*, 38, 493
Cuzzi, J. N., Hogan, R. C., Paque, J. M., & Dobrovolskis, A. R. 2001, *ApJ*, 546, 496
Fleming, T., Stone, J. M. 2003, *ApJ*, 585, 908
Goldreich, P., & Ward, W. R. 1973, *ApJ*, 183, 1051
Johansen, A., Henning, Th., & Klahr, H. 2006, *ApJ*, 643, 1219
Lee, A. T., Chiang, E., Asay-Davis, X., & Barranco, J. 2010, *ApJ*, 718, 1367
Michikoshi, S., Kokubo, E., & Inutsuka S.-i. 2012, *ApJ*, 746, 35 (MKI12)
Nakagawa, Y., Sekiya, M., & Hayashi, C. 1986, *Icarus*, 67, 375
Okuzumi, S., & Hirose, S. 2011, *ApJ*, 742, 65
Sekiya, M. 1983, *Prog. Theor. Phys.*, 69, 1116
Sekiya, M. 1998, *Icarus*, 133, 298
Shariff, K., & Cuzzi, J. N. 2011, *ApJ*, 738, 73 (SC11)
Takeuchi, T., & Lin, D. N. C. 2002, *ApJ*, 581, 1344
Takeuchi, T., Clarke, C. J., & Lin, D. N. C. 2005, *ApJ*, 627, 286
Takeuchi, T., Muto, T., Okuzumi, S., Ishitsu, N., & Ida, S. 2012, *ApJ*, 744, 101 (T12)
Tanaka, H., Himeno, Y., & Ida, S. 2005, *ApJ*, 625, 414
Ward, W. R. 2000, in *Origin of the Earth and Moon*, ed. R. M. Canup & K. Righter (Tucson, AZ: Univ. Arizona Press), 75
Weidenschilling, S. J. 2003, *Icarus*, 165, 438
Youdin, A. N. 2005a, arXiv:astro-ph/0508659
Youdin, A. N. 2005b, arXiv:astro-ph/0508662
Youdin, A. N. 2011, *ApJ*, 731, 99 (Y11)
Youdin, A. N., & Chiang, E. I. 2004, *ApJ*, 601, 1109
Youdin, A. N., & Shu, F. H. 2002, *ApJ*, 580, 494